



OPEN ACCESS

EDITED BY

Shiliang Yang,
Kunming University of Science and Technology,
China

REVIEWED BY

Yanjie Li,
Beijing Forestry University, China
Yuanhe Yue,
Hebi University of Technology, China

*CORRESPONDENCE

Numan Naeem,
✉ numan.naeem@zju.edu.cn
Jinxin Tie,
✉ tiejinxin@zjtobacco.com
Yu Guo,
✉ yguo@zju.edu.cn

RECEIVED 27 May 2025

ACCEPTED 20 June 2025

PUBLISHED 04 July 2025

CITATION

Song J, Naeem N, Fan H, Li G, Li M, Guo Y, Lin J
and Tie J (2025) Flow and mixing of elongated
particles in rotating drums of different sizes.
Front. Chem. Eng. 7:1636010.
doi: 10.3389/fceng.2025.1636010

COPYRIGHT

© 2025 Song, Naeem, Fan, Li, Li, Guo, Lin and
Tie. This is an open-access article distributed
under the terms of the [Creative Commons
Attribution License \(CC BY\)](https://creativecommons.org/licenses/by/4.0/). The use,
distribution or reproduction in other forums is
permitted, provided the original author(s) and
the copyright owner(s) are credited and that the
original publication in this journal is cited, in
accordance with accepted academic practice.
No use, distribution or reproduction is
permitted which does not comply with these
terms.

Flow and mixing of elongated particles in rotating drums of different sizes

Jinhua Song¹, Numan Naeem^{2*}, Hu Fan³, Guanhua Li¹,
Maosong Li³, Yu Guo^{2*}, Jianzhong Lin^{2,4} and Jinxin Tie^{1*}

¹Ningbo Cigarette Factory, China Tobacco Zhejiang Industrial Co., Ltd., Ningbo, China, ²Department of Engineering Mechanics, Zhejiang University, Hangzhou, China, ³Technology Center, China Tobacco Zhejiang Industrial Co. Ltd., Hangzhou, China, ⁴Zhejiang Provincial Engineering Research Center for the Safety of Pressure Vessel and Pipeline, Ningbo University, Ningbo, China

A numerical study is performed using the Discrete Element Method (DEM) to investigate flow and mixing of elongated particles in rotating drums. Spherical particles and their mixtures have been extensively explored in the previous work, while the present study focuses on the elongated rod-like particles and binary mixtures of the elongated particles with two different aspect ratios. Different drum sizes are used to examine scale-up behaviors in such dynamic processes. For both monodisperse and binary particle systems, dynamic angle of repose is determined mainly by a Froude number Fr , measuring the ratio of centrifugal force to gravitational force on a particle, while it is insensitive to scale-up ratio α , defined as the ratio of cross-sectional areas of the current drum to the reference one. Average particle velocity and contact force generally increase with both Froude number and scale-up ratio. Mixing rate of the particles is significantly promoted by increasing Fr , and it maintains constant at small Fr and decreases slowly with increasing α at large Fr . Some differences are observed between the monodisperse and binary systems: i) The mixing index eventually achieves the same high level for all the monodisperse systems, while the final mixing indices are smaller with smaller Fr for the binary systems; ii) The mixing rate of the binary mixtures has a stronger dependence on the scale-up ratio α than the monodisperse systems; iii) With increasing α , the average contact force increases for the monodisperse systems while it changes non-monotonically at large Froude numbers for the binary systems.

KEYWORDS

elongated particle, flow, mixing, scale-up, DEM

1 Introduction

In many industries such as pharmaceutical, food processing, materials engineering, and so on, mixing of solid particles, which may have different sizes, shapes and densities, is a critical process. In order to achieve efficient and reliable mixing, rotating drums are frequently used because of excellent capacity for bulk solids handling (Jiang et al., 2023; Xu et al., 2023; Dong et al., 2024). Combined with their ability of heat transfer efficiency (Figueroa et al., 2010; Gui et al., 2013), the rotating drums are applied in a broad range of industrial processes involving drying, reactions, segregation, coating, grinding, heating, and cooling operations (Trojosky, 2019; Orozco et al., 2020; Liu et al., 2024). Six different regimes (from slipping to centrifuging) have been recognized based upon a Froude number, defined as the ratio of centrifugal to gravitational forces (Beaulieu et al., 2021; Chen et al.,

2024). To obtain homogenous mixtures, the rolling and cascading regimes should be adopted (Norouzi et al., 2015). In these flow regimes, active and passive regions of particle motion are observed. In the passive region, the particles move as a rigid body, and their velocity is lower than that of the particles in the active layer. An active layer of the flowing particles is formed, when the particles reach the highest point along the wall, and then they fall like an avalanche under gravitational forces. The active layer is much thinner than the passive region, due to the existence of a yield stress for the particle flow. The mixing, segregation and heat transfer mainly happen in the active layer where the shearing rate is high (Alizadeh et al., 2013).

The outcomes of the particle mixing depend upon the size of the mixer. Many studies on the particle mixing are typically conducted at the laboratory scale, instead of industrial level. The relevance of the results obtained from the small scales to those at the large scales remains unclear (Portillo et al., 2008). A lot of studies have been done previously on various scaling conditions to determine the scale-up laws (Ding et al., 2001) that ensure similarities in dynamic behaviors of granular materials across the drums of different sizes (Govender, 2016). Various dimensionless numbers have been proposed in the scale-up studies. Recently, He et al. (2024) studied the segregation of bi-dispersed spherical particles caused by particle size difference inside different cylindrical drums, and they found that the contact forces and power consumption strongly depended on the Froude number. Herman et al. (2021) found that the similar mixing quality was achieved in a scale up process by keeping the same kinematic and dynamic similarities in bladed mixers. In their study, they used monodispersed spherical particles and proposed scaling correlations for average particle velocity (V_a) and total particle contact force (F_{ct}) can be written as:

$$V_a = 0.766Fr^{1.060}\alpha^{0.169}, \quad (1)$$

$$F_{ct} = 6.495Fr^{1.077}\alpha^{-0.077}, \quad (2)$$

in which Fr represents Froude number and α is the scale-up ratio, defined as the ratio of the volume of the current drum to the reference one. Different ribbon mixers of volumes 5.62 L–482.32 L were then used by (Herman et al., 2022a) to examine the effect of mixer sizes on the particle mixing quality, and it was found that the mixing time and power consumption to achieve the same quality were reduced in the larger mixers than the smaller ones. In their scale-up studies, (Herman et al., 2022b) investigated the mixing performance of spherical particles in different drums. Their proposed correlation for the mixing rate (R) of monodispersed spherical particles is expressed as:

$$R = 0.44Fr^{0.235}\alpha^{-0.279}. \quad (3)$$

Experimental scale-up studies of the granular flows are usually expensive and labor intensive. Also, it's very difficult to obtain the particle-scale information in the experiments for a deeper, microscopic understanding of the physical processes. To address these deficiencies, numerical approach, such as the Discrete Element Method (DEM), was used to simulate the drum rotating processes (Li et al., 2022), and the scale-up of the particulate systems in the drums was studied (Li et al., 2020). In the DEM simulations of the polyhedral particle flows (Vu et al., 2024), it was found that the

active layer depth and curvature and particle velocity could be expressed as functions of the Froude number. In the DEM studies of heat transfer in a rotary drum (Ardalani et al., 2023), it was found that a larger number of baffles installed inside the drum led to a higher rate of heat transfer, while the temperature distributions of the particles and bed uniformity were unaffected by the changes in the baffle number.

Most grains and particles in the industries have non-spherical shapes (Ma et al., 2022). Flow patterns of the particles with anisotropic shapes are more complex at various rotational speeds of the drums (Yang et al., 2008). The non-spherical particle shapes give rise to segregation (Yang et al., 2017; Kumar et al., 2024; Miao et al., 2024), and thus influence the mixing performance (He et al., 2020). In the studies of the rotating drums, elongated, rod-like particles gained interests of many researchers (Yu et al., 2018; Yu et al., 2020), because of their important applications in fibrous materials (Rudge et al., 2008) and pharmaceuticals (Kodam et al., 2012). As the motion of the rod-like particles is more restrained inside the drum due to interlocking particle-particle contacts (Li et al., 2021), their dynamics and mixing behaviors are different from the spherical particles. Some open questions are still remaining in the rotating drums of the rod-like particles. For instance, how are the particle flow and mixing patterns and quantities influenced when the drum size is changed? Do the rod-like particles have different scale-up behaviors from the spherical particles?

This work aims to address these questions by performing the DEM simulations. The flow and mixing of monodisperse and binary elongated, rod-like particles in the rotating drums of different sizes are simulated. The scale-up behaviors are discussed for angle of repose, particle mixing rate, average particle velocity, and contact forces.

2 Computational set-up

2.1 Discrete element method

In the Discrete Element Method (DEM), an elongated particle is represented by a sphero-cylinder. Each particle is considered as a discrete entity and its translational and rotational motion in Equations 4, 5 is described by Newton's second law of motion,

$$m_i \frac{d\mathbf{v}_i}{dt} = \mathbf{F}_i + m_i \mathbf{g}, \quad (4)$$

$$\mathbf{I}_i \frac{d\boldsymbol{\omega}_i}{dt} - (\mathbf{I}_i \cdot \boldsymbol{\omega}_i) \times \boldsymbol{\omega}_i = \mathbf{M}_i, \quad (5)$$

where translational and angular velocities of the particle i of the mass m_i are represented by \mathbf{v}_i and $\boldsymbol{\omega}_i$, respectively, \mathbf{g} is gravitational acceleration, and \mathbf{F}_i is the resultant contact force exerted on the particle i . The moment of inertia tensor of the particle i is represented by \mathbf{I}_i and \mathbf{M}_i is the total torque produced by the contact forces on the particle i .

The resultant contact force between a particle and another particle or a wall boundary can be decomposed into a normal contact force and a tangential one. In this work, the normal contact force \mathbf{F}_n^c follows a linear spring dashpot model,

$$\mathbf{F}_n^c = k_n \delta_n \mathbf{n} - C_n \mathbf{v}_n, \quad (6)$$

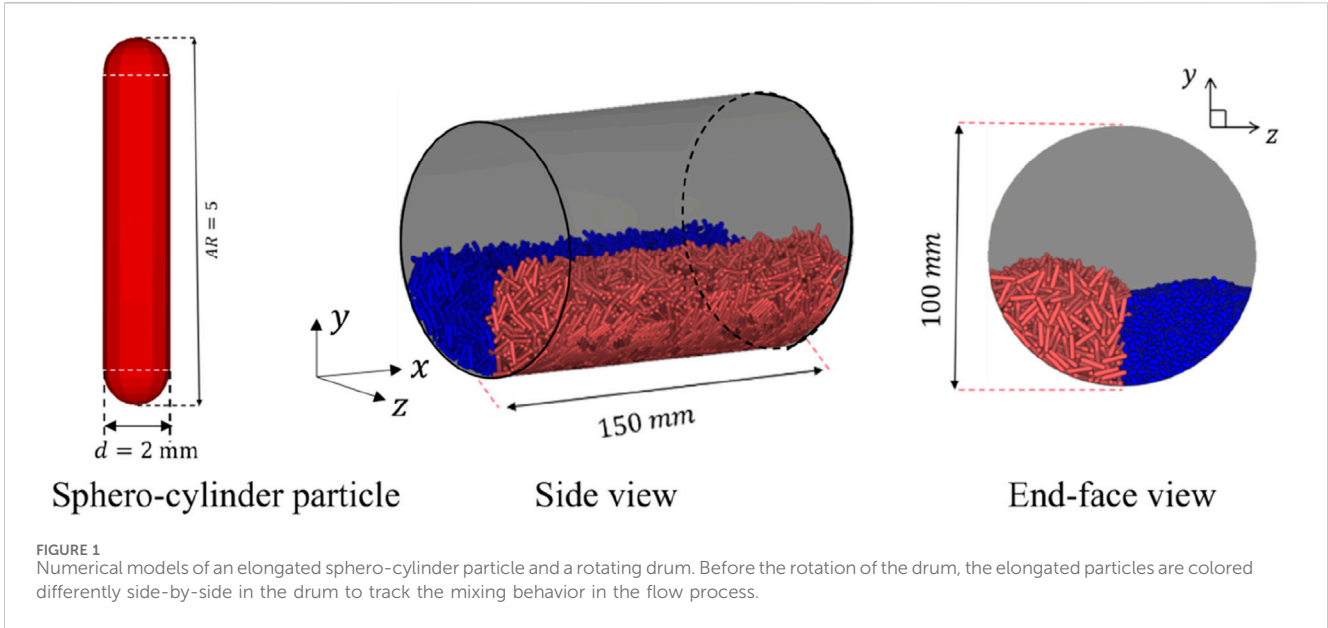


FIGURE 1 Numerical models of an elongated sphero-cylinder particle and a rotating drum. Before the rotation of the drum, the elongated particles are colored differently side-by-side in the drum to track the mixing behavior in the flow process.

in which the normal contact stiffness k_n in Equation 7 is written as,

$$k_n = \frac{E_i d_i \cdot E_j d_j}{E_i d_i + E_j d_j} \tag{7}$$

and d_i and d_j denotes diameters of the two contacting sphero-cylinder particles i and j , E_i and E_j are Young's moduli, respectively, of the two particles, δ_n represents contacting overlap size, and \mathbf{n} is the unit vector of the contact normal direction. The second term of the right hand side of Equation 6 accounts for the collisional dissipation of energy, in which $C_n = 2\beta \sqrt{m^* k_n}$ is the normal damping coefficient, $m^* = \frac{m_i m_j}{m_i + m_j}$ is the effective mass, and \mathbf{v}_n is the normal relative velocity vector at the contact point.

Linear spring-dashpot Coulomb limit model (Zhu et al., 2007) is employed to calculate tangential contact force at time t , in Equations 8, 9 expressed as $\mathbf{F}_\tau^{c,t}$.

$$\mathbf{F}_\tau^{c,t} = \min \left(|\mathbf{F}_{\tau,e}^{c,t}|, \mu |\mathbf{F}_n^{c,t}| \right) \frac{\mathbf{F}_{\tau,e}^{c,t}}{|\mathbf{F}_{\tau,e}^{c,t}|} \tag{8}$$

in which,

$$\mathbf{F}_{\tau,e}^{c,t} = \mathbf{F}_\tau^{c,t-\Delta t} - K_\tau \mathbf{v}_\tau \Delta t - C_\tau \mathbf{v}_\tau, \tag{9}$$

and μ is the particle-particle or particle-wall friction coefficient, $\mathbf{F}_n^{c,t}$ is the normal contact force at time t , $\mathbf{F}_\tau^{c,t-\Delta t}$ is the tangential contact force for the previous time step, K_τ is the tangential contact stiffness, \mathbf{v}_τ is the relative tangential velocity vector at the contact point, Δt is the time step, and C_τ is the tangential damping coefficient. When $|\mathbf{F}_{\tau,e}^{c,t}| < \mu |\mathbf{F}_n^{c,t}|$, it is in static friction stage, otherwise it is in dynamic or sliding friction stage.

2.2 Numerical model

The dynamics of elongated sphero-cylinder particles in a rotating drum is simulated. As shown in Figure 1, the particles have a diameter of $d = 2$ mm and lengths of $l_p = 4$ mm and 10 mm,

TABLE 1 Particle properties used in the DEM simulations.

Parameters	Value
Particle diameter (d), mm	2
Aspect ratio (AR)	2 and 5
Poisson's ratio (ν)	0.3
Coefficient of restitution (e)	0.3
Material density (ρ), kg/m^3	264
Friction coefficient for particle-particle contacts (μ_{pp})	0.4
Friction coefficient for particle-wall contacts (μ_{pw})	0.7
Young's modulus (E), Pa	1×10^8
Time step (Δt), s	3.893×10^{-7} and 6.541×10^{-7}

resulting in the particle aspect ratios of $AR = l_p/d = 2$ and 5, respectively. Monodisperse particles with $AR = 5$ or binary particle mixtures of $AR = 2$ and five settle under gravitational forces to densely-packed assemblies in the cylindrical drum of a diameter of $D = 100$ mm and length of $L = 150$ mm (Figure 1), before the drum rotates at a specified angular speed about its major axis in the x -direction. The particle properties used for the DEM simulations are listed in Table 1. The choices of the particle properties are based on the biomass materials as reported in (Han et al., 2023).

To examine scale-up rules for the present drum systems, four drums of different diameters, i.e. Drum A to D, are used in the simulations, as shown in Table 2. As the flow patterns and mixing behaviors show no dependences on it, the length of the drum L remains the same for the four drums. To achieve the similarity of the system, the same fill ratio, defined as the total volume of the particles to the volume of the drum, is specified to the four drums, for which the number of particles increases linearly with the volume of the

TABLE 2 Simulation conditions of four drums of different diameters.

Drum	A	B	C	D
Diameter (D), mm	100	115	130	145
Length (L), mm	150	150	150	150
Number of particles (monodisperse, $AR = 5$)	8,574	11,340	14,488	18,032
Number of particles (binary mixture, $AR = 2$ and $AR = 5$)	16,289	21,546	27,526	34,261
Scale-up ratio (α)	1	1.3	1.7	2.1

TABLE 3 Rotational speeds (unit in rpm) of four different drums at various Froude numbers (Fr).

Drum	Froude number (Fr)			
	0.05	0.1007	0.50	1.10
A	21.14	30.00	66.85	99.15
B	19.71	27.97	62.33	92.46
C	18.54	26.31	58.63	86.96
D	17.55	24.91	55.51	82.34

drum. The monodisperse particles have particle aspect ratio of $AR = 5$. The binary mixtures are composed of two components with $AR = 2$ and $AR = 5$, respectively, and both components have volume concentrations of 50% in the mixtures. For the drum systems, a scale-up ratio α is defined as the ratio of cross-sectional area of the current drum ($\pi D^2/4$) to that of the reference drum. In the present study, Drum A is the reference drum and thus, α spans between 1 and 2.1.

A Froude number (Fr) in Equation 10, reflecting the relative importance of centrifugal and gravitational forces on a particle, can be written as

$$Fr = \frac{D\omega^2}{g}, \quad (10)$$

in which ω is the rotational speed of the drum and $D\omega^2$ scales with the centrifugal force on a particle, and g is the gravitational acceleration scaling with the gravitational force. Four different Froude numbers are used and corresponding rotational speeds of the drums are listed in Table 3.

2.3 Lacey mixing index

Various mixing indices exist and it is critical to choose a proper one to describe the degree of particle mixing for a specific process (Bhalode and Ierapetritou, 2020). The Lacey mixing index (Lacey, 1954) L has been widely used to quantify the mixing degree in various solids handling processes, including in a rotating drum, and it is calculated as,

$$L = \frac{S_0^2 - S^2}{S_0^2 - S_R^2}, \quad (11)$$

in which,

$$S_0^2 = x(1-x), \quad (12)$$

$$S_R^2 = \frac{x(1-x)}{n}, \quad (13)$$

$$S^2 = \frac{1}{N-1} \sum_{i=1}^N (x_i - x)^2. \quad (14)$$

In the calculation, the whole particle system is partitioned into many subdomains, namely boxes. The variances of an initial mixing state and a completely mixed state are represented by S_0^2 and S_R^2 , respectively, and the current mixing state is S^2 . In Equations 12–14, x is the overall concentration of tracer particles in the whole system, n is the average number of particles in each box, N is the number of the boxes, and x_i is the concentration of the tracer particles in the current box i . The lacey mixing index L runs within $[0, 1]$, in which 0 represents the completely unmixed state and 1 represents the fully mixed state.

3 Monodisperse system of elongated particles

3.1 Dynamic angle of repose

A slope of particles with a wavy surface is formed in the rotating drum, as shown in Figure 2. Larger curvature of the granular surface is obtained for the elongated particles compared to the spherical particles (Cui et al., 2023). To describe the particle flow patterns, the profile of the granular surface is fitted using a straight line. The inclination angle of the straight line θ (Figure 2a) is defined as the dynamic angle of repose, which fluctuates slightly around an average value at the steady flow stage. For a given Froude number Fr , the average dynamic angle of repose is independent on the scale-up ratio α for $\alpha \in [1, 2.1]$, as shown in Figure 2b. In a drum of a specified scale-up ratio α , the average dynamic angle of repose changes slightly with the Froude number Fr for $Fr \leq 0.5$, while a surge of about 10° in the average θ is obtained as Fr increases from 0.5 to 1.1. This sharp increase at $Fr = 1.10$ is attributed to the change in the flow regimes caused by stronger centrifugal effect at a higher rotation speed of the drum. Thus, the average dynamic angle of repose is basically determined by the Froude number for the drums of various sizes.

3.2 Particle velocities

Different particle flow regimes can be observed in the drums, as shown in Figure 3. The particles have higher velocities as they

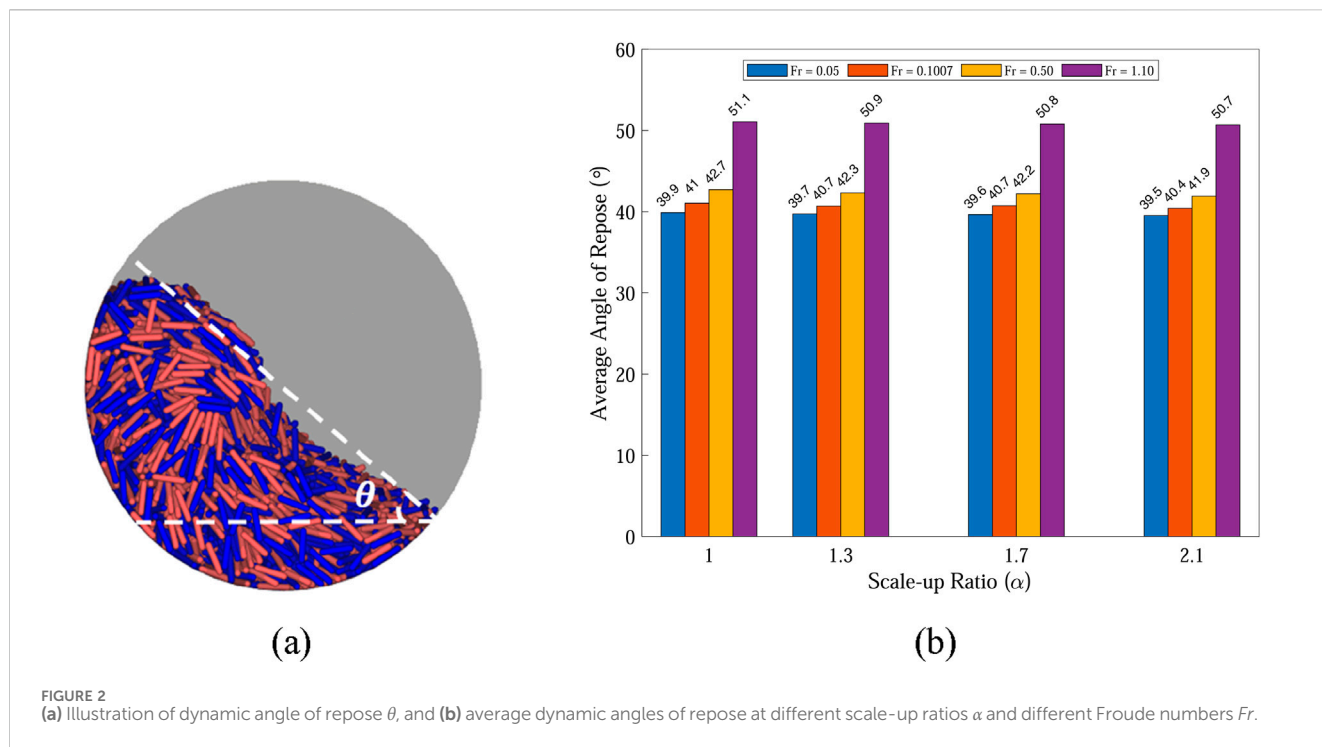


FIGURE 2 (a) Illustration of dynamic angle of repose θ , and (b) average dynamic angles of repose at different scale-up ratios α and different Froude numbers Fr .

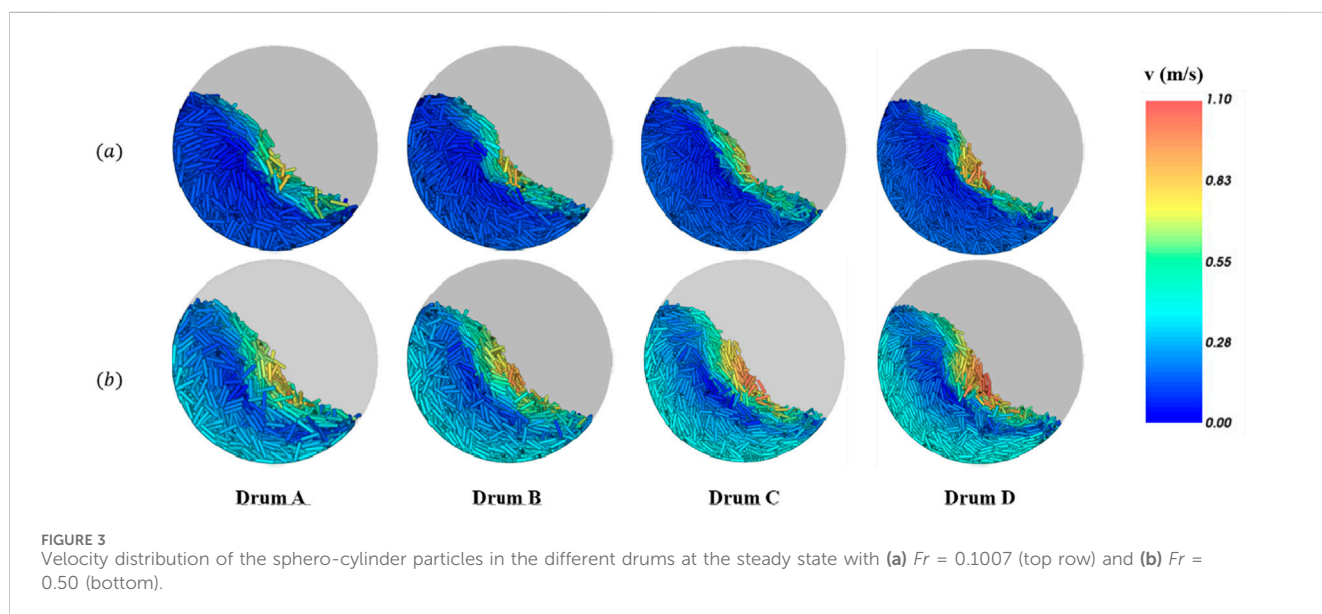


FIGURE 3 Velocity distribution of the sphero-cylinder particles in the different drums at the steady state with (a) $Fr = 0.1007$ (top row) and (b) $Fr = 0.50$ (bottom).

cascade down on the curved surface. The particles contacting the inner surface of the drum generally have the same velocities to the surface (like non-slip boundary), and thus their velocities increase with increasing Froude number Fr for a given drum. Low-velocity regimes are formed in the centers of the circulating particle assemblies.

The probability distributions of the particle velocities are shown in Figure 4. Low particle velocities correspond to the central region. Intermediate velocities correspond to the boundary layer of the particles contacting the rotating wall,

and thus the peak probability occurs at a higher particle velocity in a larger drum. The long tail in a probability distribution curve at the higher particle velocities (particle velocities are greater than 0.2 m/s in Figure 4a and greater than 0.4 m/s in Figure 4b) is associated with the rapid flowing particle surface region, in which shear rates are higher and velocity distribution is wider.

For a given Froude number Fr , the average particle velocity increases with the scale-up ratio α , as shown in Figure 5a, and this velocity increase becomes more significant as Fr increases. A power

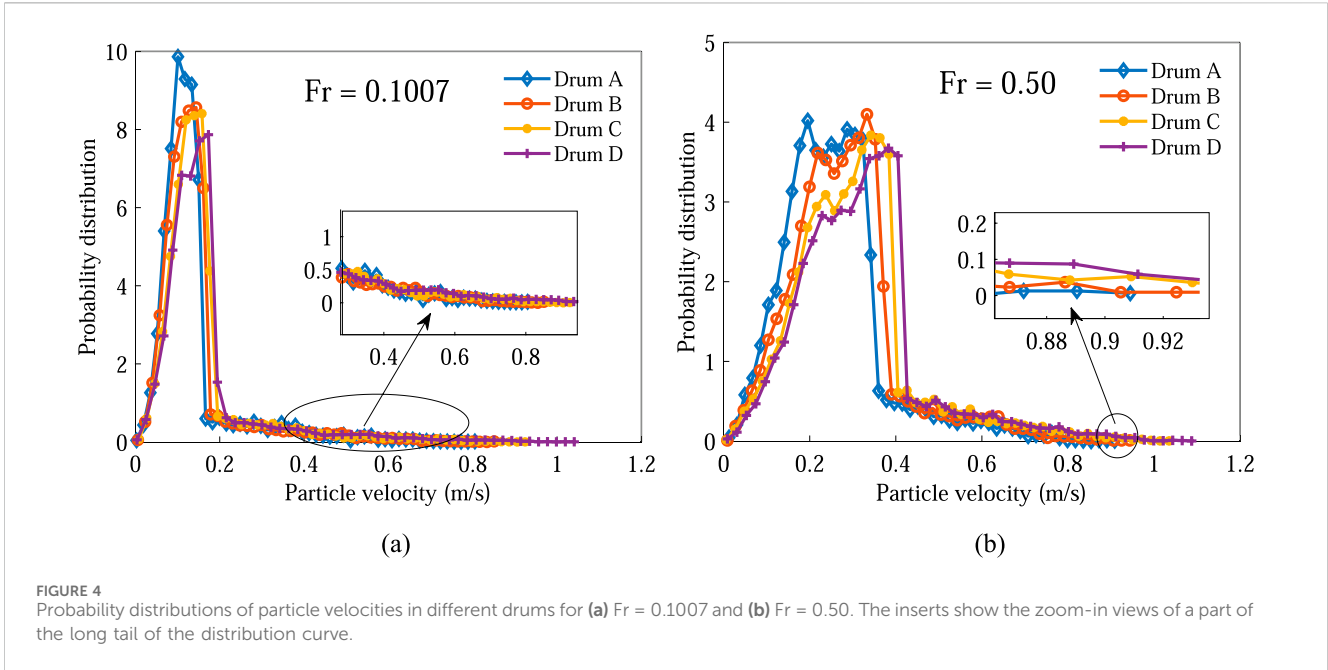


FIGURE 4 Probability distributions of particle velocities in different drums for (a) $Fr = 0.1007$ and (b) $Fr = 0.50$. The inserts show the zoom-in views of a part of the long tail of the distribution curve.

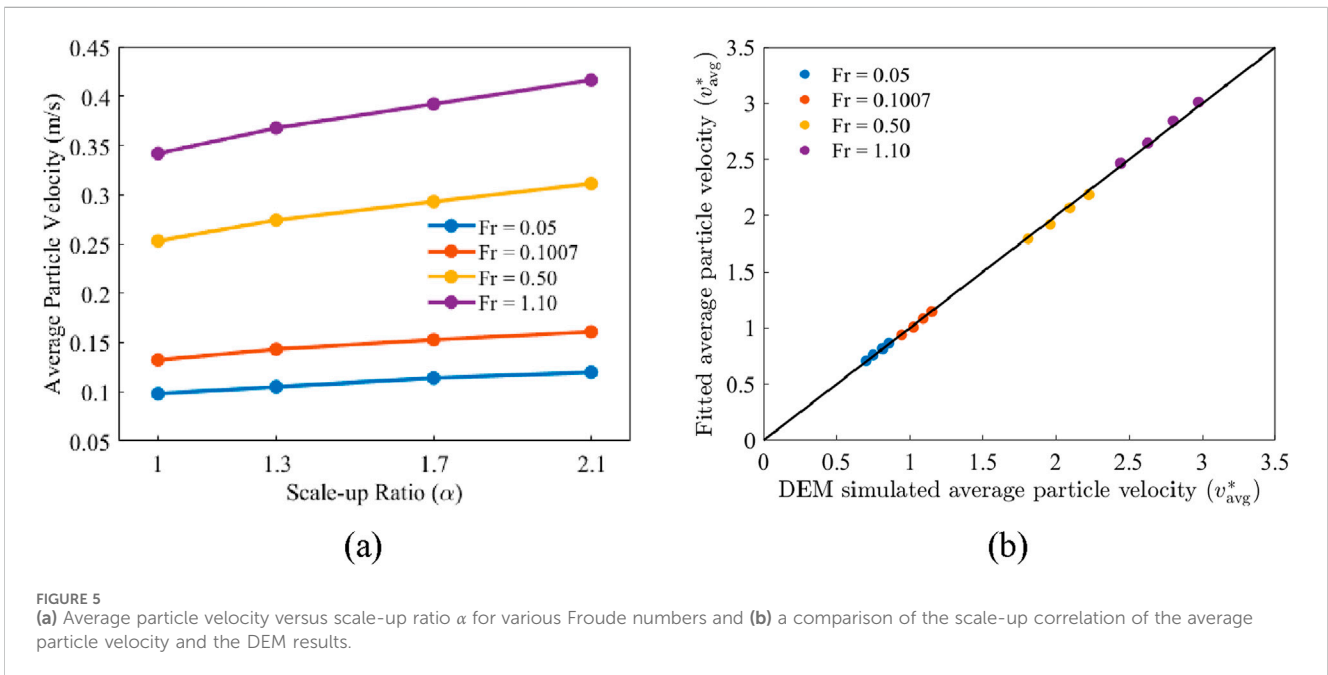


FIGURE 5 (a) Average particle velocity versus scale-up ratio α for various Froude numbers and (b) a comparison of the scale-up correlation of the average particle velocity and the DEM results.

law relationship is proposed to estimate the dependence of the average particle velocity v_{avg} on Fr and α , and it is determined by fitting to the data in Figure 5a,

$$v_{avg}^* = \frac{v_{avg}}{\sqrt{gd_p}} = 2.374 Fr^{0.4039} \alpha^{0.2686} \quad (15)$$

in which v_{avg}^* is a dimensionless average particle velocity expressed as $v_{avg}/\sqrt{gd_p}$. The predictions of Equation 15 are compared with the DEM simulation results in Figure 5b, and a good agreement is observed.

3.3 Contact forces on the particles

The contact forces exerted on the particles due to particle-particle and particle-wall contacts determine attrition and breakage of the particles and erosion on the drum walls. The average contact force exhibits significant increase as both scale-up ratio α and Froude number Fr increase, as depicted in Figure 6a. In general, higher particle velocities lead to larger contact forces. Thus, the trend of the contact force varying with Fr and α is correlated with that of the average particle velocity (Figure 5a). A

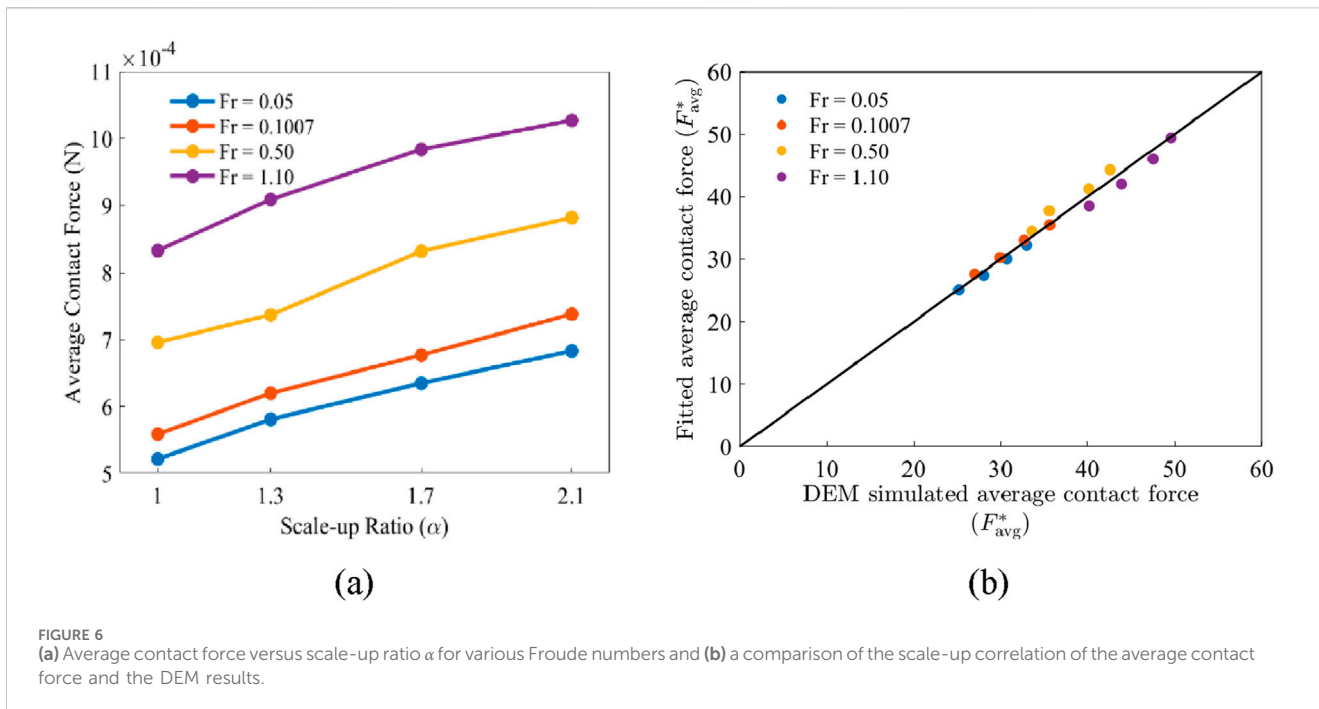


FIGURE 6 (a) Average contact force versus scale-up ratio α for various Froude numbers and (b) a comparison of the scale-up correlation of the average contact force and the DEM results.

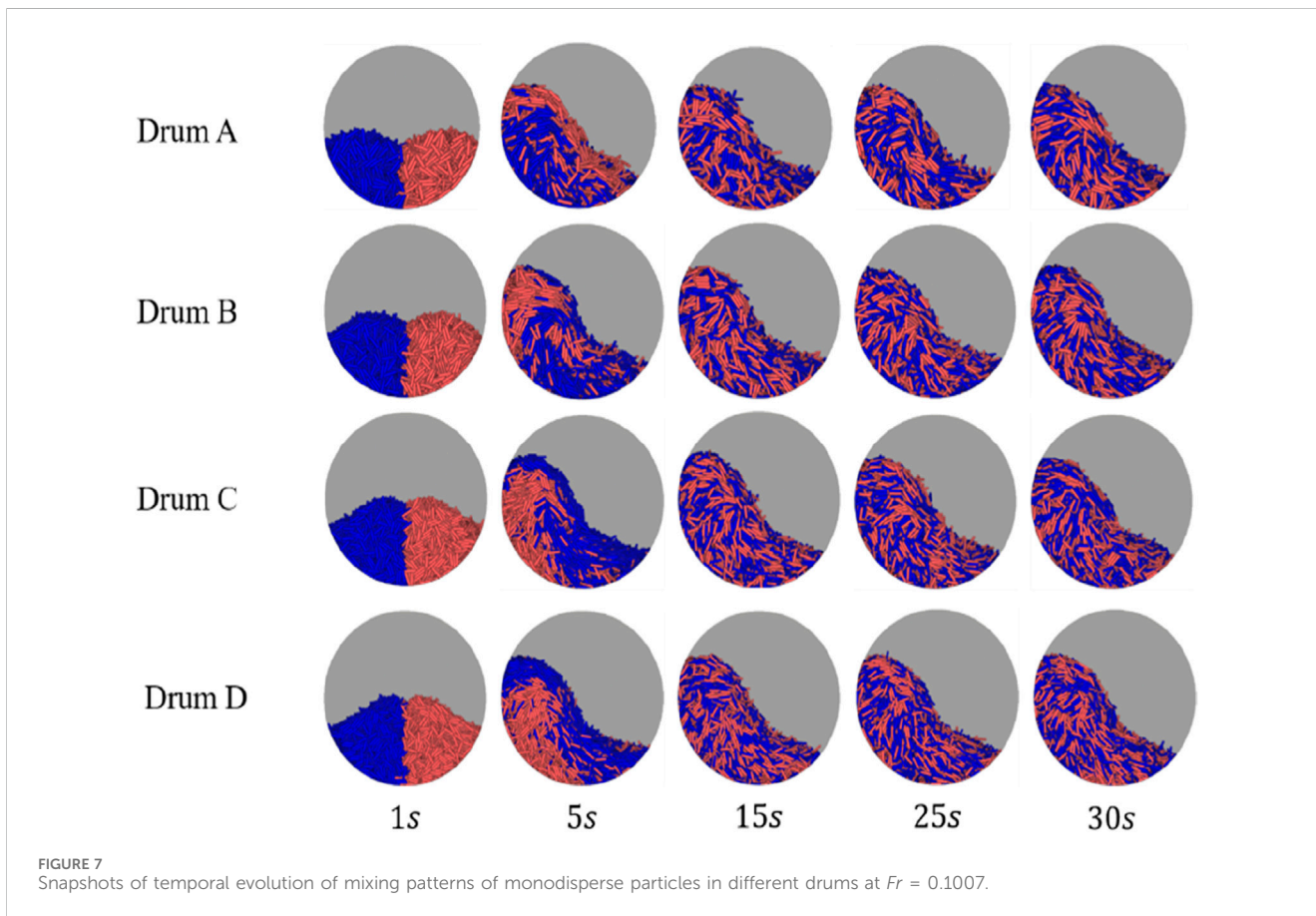


FIGURE 7 Snapshots of temporal evolution of mixing patterns of monodisperse particles in different drums at $Fr = 0.1007$.

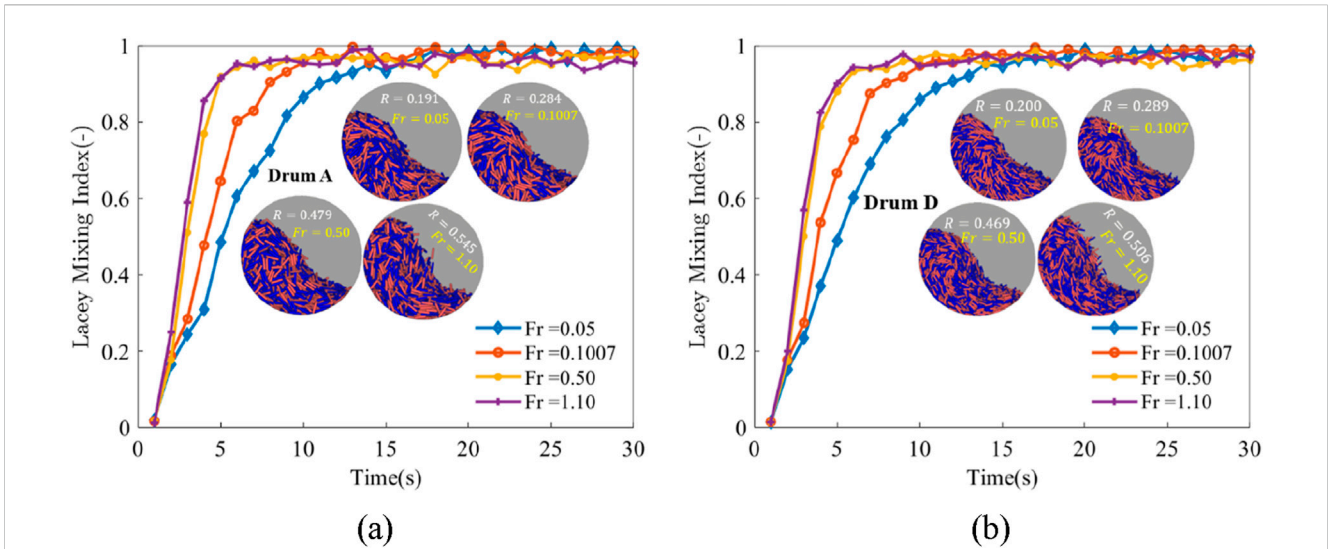


FIGURE 8 Time evolution of Lacey mixing index L at various Froude numbers Fr in (a) Drum A and (b) Drum D. The inset images show the mixed particle patterns at $t = 30$ s and the mixing rates R for the four Froude numbers.

power law relationship, which correlates the average contact force F_{avg} , Fr and α , is determined by fitting to the data in Figure 6a,

$$F_{avg}^* = \frac{F_{avg}}{\rho g d_p^3} = 37.97 Fr^{0.1383} \alpha^{0.3368} \quad (16)$$

in which F_{avg}^* is a dimensionless average contact force expressed as $F_{avg}/(\rho g d_p^3)$. The prediction of Equation 16 is generally consistent with the DEM results, as shown in Figure 6b.

3.4 Mixing performance

To observe and quantify the mixing behavior, the monodisperse particles are partitioned equally in number and colored differently in blue (left-hand side) and red (right-hand side), as shown in Figure 7. To ensure the consistent particle loading, two rectangular inlet regions with the fixed dimensions were used in all drum. However, as the drum cross-sectional area increases, the relative inlet area becomes smaller, leading to slight variations in the initial packing profile at $t = 1$ s (Figure 7). In the four drums of different sizes (Drums A-D), similar flow and mixing patterns are observed at the same Froude number of $Fr = 0.1007$ (Figure 7). Lacey mixing index L , calculated by Equation 11, initially increases with time, then converges to an upper limit, and eventually fluctuates around a constant value for various Fr in different drums, as shown in Figure 8. For a given drum (Figure 8a or Figure 8b), the convergence to the upper limit of the mixing index L occurs earlier at a larger value of Fr , because the higher rotational speed of the drum ω promotes the convective particle flow and thus mixing in the present flow regime in the drum.

According to Figure 8, the Lacey mixing index L and elapsed time t follow an error function (Herman et al., 2022a; He et al., 2024) in the form,

$$L = L_f + (L_0 - L_f) \exp(-Rt), \quad (17)$$

in which $\exp(-)$ represents the exponential function, L_f is the upper limit of the Lacey mixing index, and L_0 is the initial mixing index before the drum rotation. The coefficient R before the time t reflects how fast the material is mixed and it is defined as mixing rate.

Fitting to the Lacey index $L-t$ curves (Figure 8) using Equation 17, the mixing rate R can be determined for each mixing process. As shown in Figure 9a, the mixing rate R is almost independent on the scale-up ratio α at lower values of Froude numbers ($Fr = 0.05 \sim 0.5$) while R decreases slightly with α at the larger value of $Fr = 1.10$. Therefore, when the drums rotate slowly (at small Fr), the mixing rate R is determined by the particle flow pattern and less affected by the drum size; when the drum rotates at a high speed or a larger Fr , the rate of particle mixing is reduced by increasing the drum size or scale-up ratio, since the particles need to move a longer distance for the same mixing outcome in a drum with larger space. In addition, for a given drum, R shows a significant increase with increasing Fr , consistent with the observation in Figure 8, due to the mixing promotion by the higher rotational speed of the drum.

By fitting to the data in Figure 9a, a power law is determined to correlate the mixing rate R , Froude number Fr , and scale-up ratio α as follows,

$$R^* = R \sqrt{\frac{d_p}{g}} = 0.0079 Fr^{0.3084} \alpha^{-0.0250}, \quad (18)$$

which indicates that α has a limited impact on the dimensionless mixing rate R^* ($=R\sqrt{d_p/g}$) as the magnitude of the exponent above it is very small, and R^* is determined mainly by Fr above which the magnitude of the exponent is much larger. A comparison of the scale-up correlation of the mixing rate (Equation 18) and the DEM results is shown in Figure 9b. The accuracy of the prediction of the mixing rate R^* based on Equation 18 is less satisfactory than those of the predictions of average particle velocity v_{avg}^* (Figure 5b) and contact force F_{avg}^* (Figure 6b), probably due to the complex nature of the mixing process involving both convection and diffusion of the

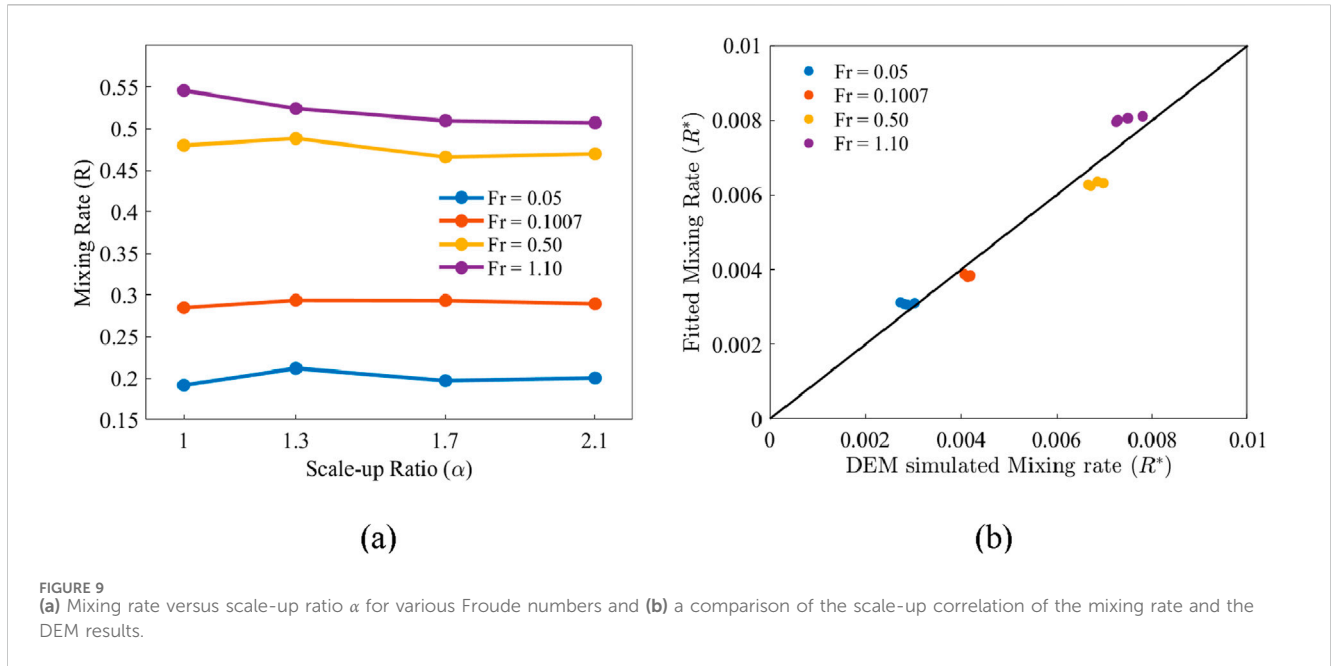


FIGURE 9 (a) Mixing rate versus scale-up ratio α for various Froude numbers and (b) a comparison of the scale-up correlation of the mixing rate and the DEM results.

particle motion, making the remarkable fluctuations in the mixing index L .

For the spherical particles, the average particle velocity V_a exhibits a more significant dependence on Fr than α , as the exponent of Fr is much larger than that of α in Equation 1. For the elongated particles, the normalized average particle velocity v_{avg}^* also depends more on Fr than α , while the difference in the exponents of Fr and α in Equation 15 is reduced compared to that for the spherical particles. The total contact force F_{ct} depends more on Fr than α for the spherical particles (Equation 2), while the average contact force F_{avg}^* depends less on Fr than α for the elongated particles (Equation 16). The mixing rate R exhibits a comparable dependence on Fr and α for the spherical particles (Equation 3), while the dimensionless mixing rate R^* has a much stronger dependence on Fr than α for the elongated particles (Equation 18).

4 Binary mixtures of elongated particles

The scale-up behaviors of monodisperse systems of the elongated particles with $AR = 5$ in the drums of different sizes are investigated in the previous section (Section 3). In this section, we aim to examine the scale-up behaviors of binary mixtures in rotating drums, and we will explore the links and differences between the monodisperse and binary systems. In the present simulation studies, the binary mixtures are composed of two particle components with $AR = 2$ and $AR = 5$, respectively, and each component occupies a volume concentration of 50% in the mixtures. The particle properties and drum parameters are listed in Tables 1, 2.

4.1 Dynamic angle of repose

For the binary mixtures of the elongated particles, the average dynamic angle of repose θ is independent on the scale-up ratio α but

shows a significant increase with increasing Froude number Fr , as demonstrated in Figure 10. Such θ -dependence on α and Fr is consistent with that of the monodisperse system (Figure 2B), indicating that the monodisperse and binary systems have the same scale-up behavior for the dynamic angle of repose.

4.2 Particle velocities

Figure 8a shows the relationship between average particle velocity, scale-up ratio, and Froude number for different drums. It can be observed that the particle velocities improve with the increase in Froude number at a constant drum scale-up ratio. It's due to the larger speed of the drum because the dominance of centrifugal forces becomes higher than the inertial forces, and particles are pushed to the drum's wall easily which enhances the particle's velocity inside the drum. Furthermore, the average velocity of particles increases with the scale-up ratio, it's because of drum diameter. Figure 8b shows the comparison plot between DEM simulated velocities and the Fitted velocities of the particles inside the different drums at different Froude number using the following power function:

For the binary mixtures, the average particle velocity v_{avg} increases with the scale-up ratio α and Froude number Fr (Figure 11a). By fitting to the data in Figure 11a, the power law relationship of the dimensionless average particle velocity v_{avg}^* ($=v_{avg}/\sqrt{gd_p}$), Fr and α is obtained as,

$$v_{avg}^* = 2.398 Fr^{0.4099} \alpha^{0.2569}. \quad (19)$$

The parameters in Equation 19 are close to those in Equation 15, indicating that the monodisperse and binary systems have the similar scale-up behaviors of the average particle velocities. A very agreement is obtained between the predictions by Equation 19 and the DEM results, as shown in Figure 11b.

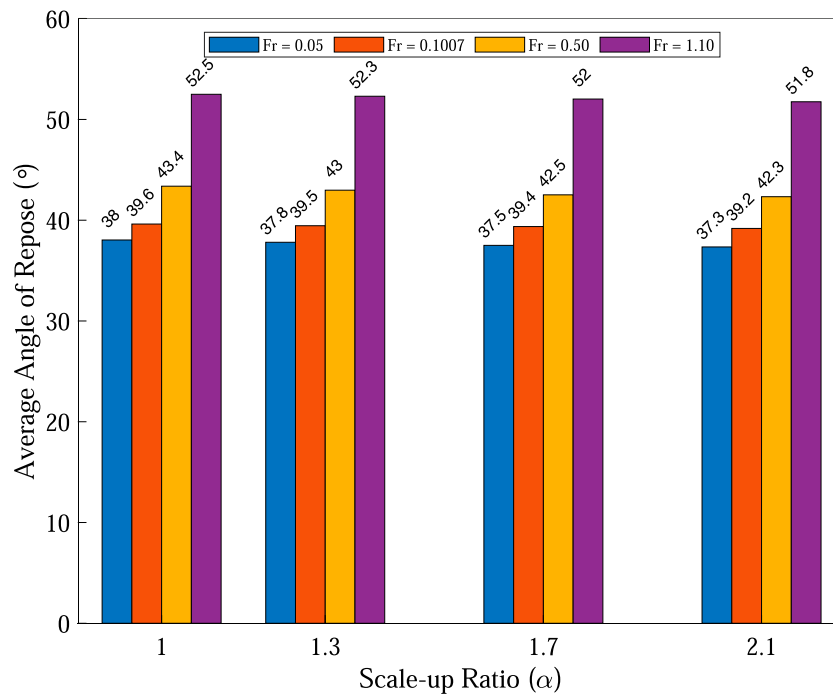
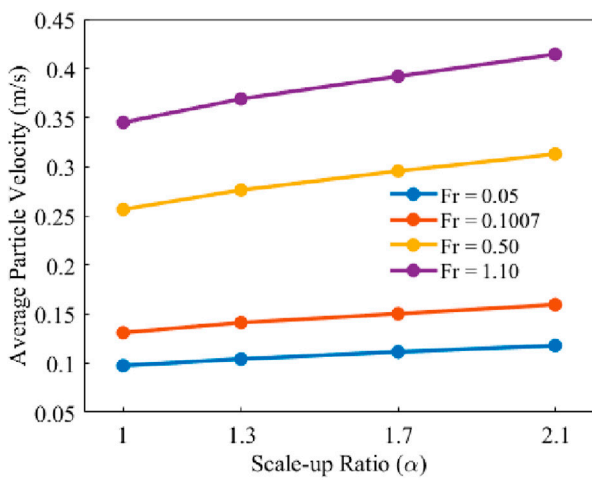
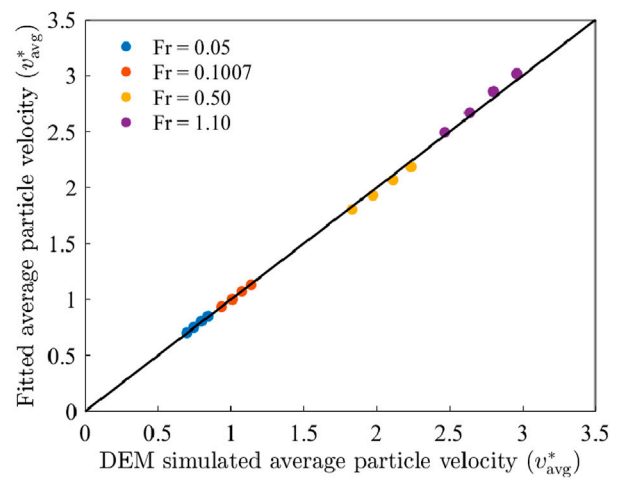


FIGURE 10 Average dynamic angle of repose of the binary mixtures at different scale-up ratios α and different Froude numbers Fr .



(a)



(b)

FIGURE 11 (a) Average particle velocity versus scale-up ratio α for various Froude numbers and (b) a comparison of the scale-up correlation of the average particle velocity and the DEM results for the binary mixtures.

4.3 Contact forces on the particles

As shown in Figure 12a, the average contact force increases with increasing scale-up ratio α at smaller Froude numbers of $Fr = 0.05$ and 0.1007 , while it changes nonmonotonically with α at larger Froude numbers of $Fr = 0.50$ and 1.10 . The interlocking structures are more likely formed in smaller drums (having smaller α) due to space

constraint. Thus, larger contact forces are obtained with $\alpha = 1$ for $Fr = 0.50$ and 1.10 . The increase of the contact force with increasing α is attributed to the increase in the average particle velocity for $\alpha > 1.3$. Fitting to the data of Figure 12 gives the power law correlation for the dimensionless contact force F_{avg}^* ($=F_{avg}/\rho g d_p^3$),

$$F_{avg}^* = \frac{F_{avg}}{\rho g d_p^3} = 35.94 Fr^{0.2231} \alpha^{0.1117}. \quad (20)$$

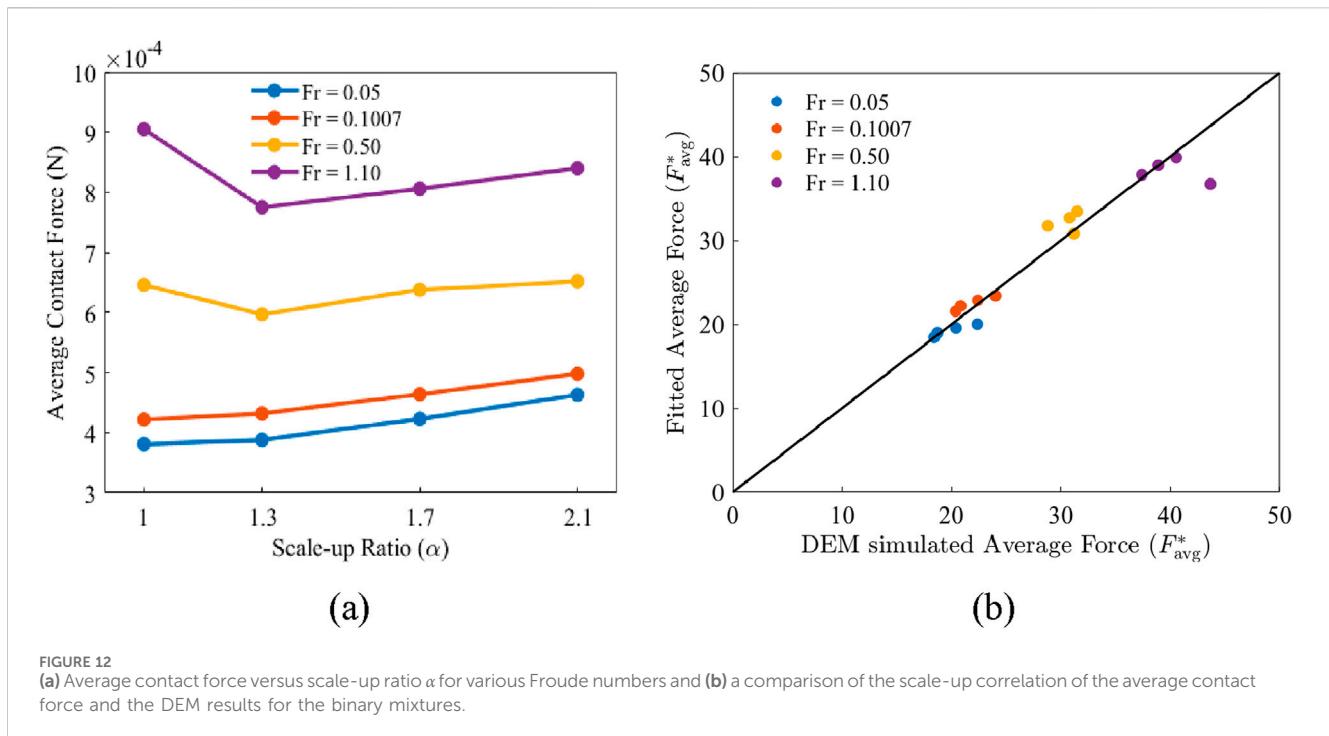


FIGURE 12 (a) Average contact force versus scale-up ratio α for various Froude numbers and (b) a comparison of the scale-up correlation of the average contact force and the DEM results for the binary mixtures.

Some predictions of the average contact forces by Equation 20 show significant deviations from the DEM results (Figure 12b), as the deviations originate from the non-monotonic changes of the contact force with increasing scale-up ratio at the high Froude numbers.

4.4 Mixing performance

In the binary mixtures, the longer particles with $AR = 5$ are colored in red and the shorter particles with $AR = 2$ in blue. The flow and mixing processes of the binary mixtures in the four different drums are shown in Figure 13. From the perspective of the radial view (the view direction parallel to the axis of the cylindrical drum), similar piling and mixture patterns are observed in the four drums. From the axial view (the view direction perpendicular to the axis of the cylindrical drum), the mixing is uniform in the axial direction of the Drum B, and such uniform mixing in the axial direction is observed in all the four drums. The radial and angular mixing is dominant in the present rotating drums.

In the circulating flows of the binary mixtures, the Lacey mixing index L increases over time before it reaches and fluctuates around an upper limit, as shown in Figure 14. The time duration required to achieve the upper limit decreases with increasing Froude number Fr . It is also observed that the upper limit of L increases with Fr for the binary mixtures (Figure 14), which is different from the monodisperse systems for which the upper limit of L is independent on Fr (Figure 8). The eventual mixing index L of the monodisperse particles is very close to 1, while the eventual L of the binary mixtures at $Fr = 0.05$ is only about 0.8. Thus, the particle size difference in the binary mixtures prevents the mixing of the two particle components, and the mixing can be improved by increasing Fr (i.e. rotational speed for a given drum).

Like the monodisperse particles (Figure 9a), for the binary mixtures (Figure 15a), the mixing rate R is nearly independent on the scale-up ratio α at lower values of Froude numbers ($Fr = 0.05 \sim 0.5$) while R decreases with α at the larger value of $Fr = 1.10$. By fitting to the data of Figure 15a, the scale-up correlation of the dimensionless mixing rate R^* ($=R\sqrt{d_p/g}$) in terms of the Froude number Fr and scale-up ratio in Figure 15b α can be written in a power law relationship,

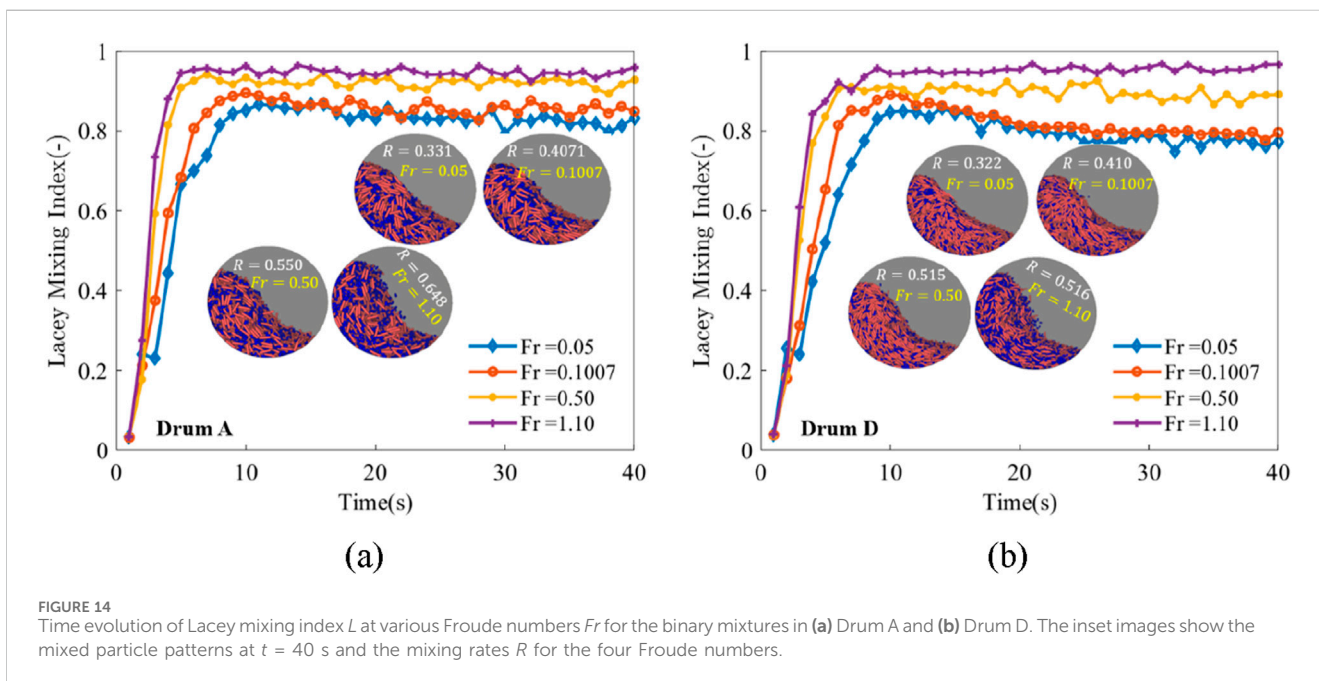
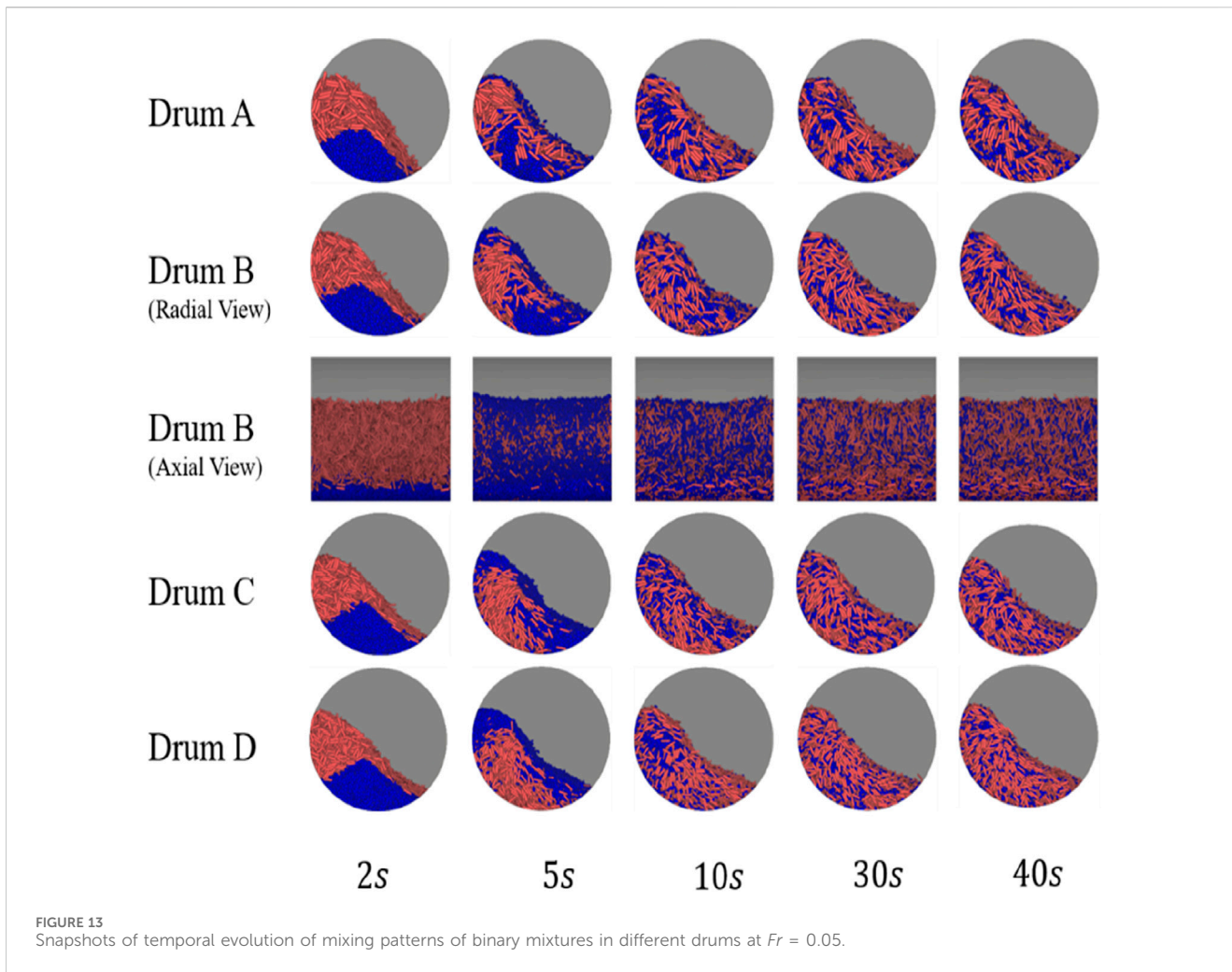
$$R^* = 0.0087 Fr^{0.1687} \alpha^{-0.1115}. \quad (21)$$

Compared to the correlation of the monodisperse system (Equation 18), the magnitude of the exponent above α in Equation 21 is much larger than that in Equation 18. Hence, the mixing rate of the binary mixtures R has a stronger dependence on the scale-up ratio α than the monodisperse systems.

5 Conclusion

In this work, flow and mixing of elongated particles in rotating drums is numerically investigated using the Discrete Element Method (DEM). The scale-up behaviors of dynamic angle of repose, particle velocity, contact force, and mixing ratio have been examined by adopting four drums of different sizes. Similarities and differences in the dynamics, mixing, and scale-up rules between monodisperse and binary particle systems are discussed. Some conclusions are drawn as follows.

- The dynamic angle of repose is determined mainly by Froude number Fr while it is insensitive to scale-up ratio α for both the monodisperse and binary systems of elongated particles.
- The scaling correlations based on Fr and α are significantly different between the spherical particles and elongated rod-



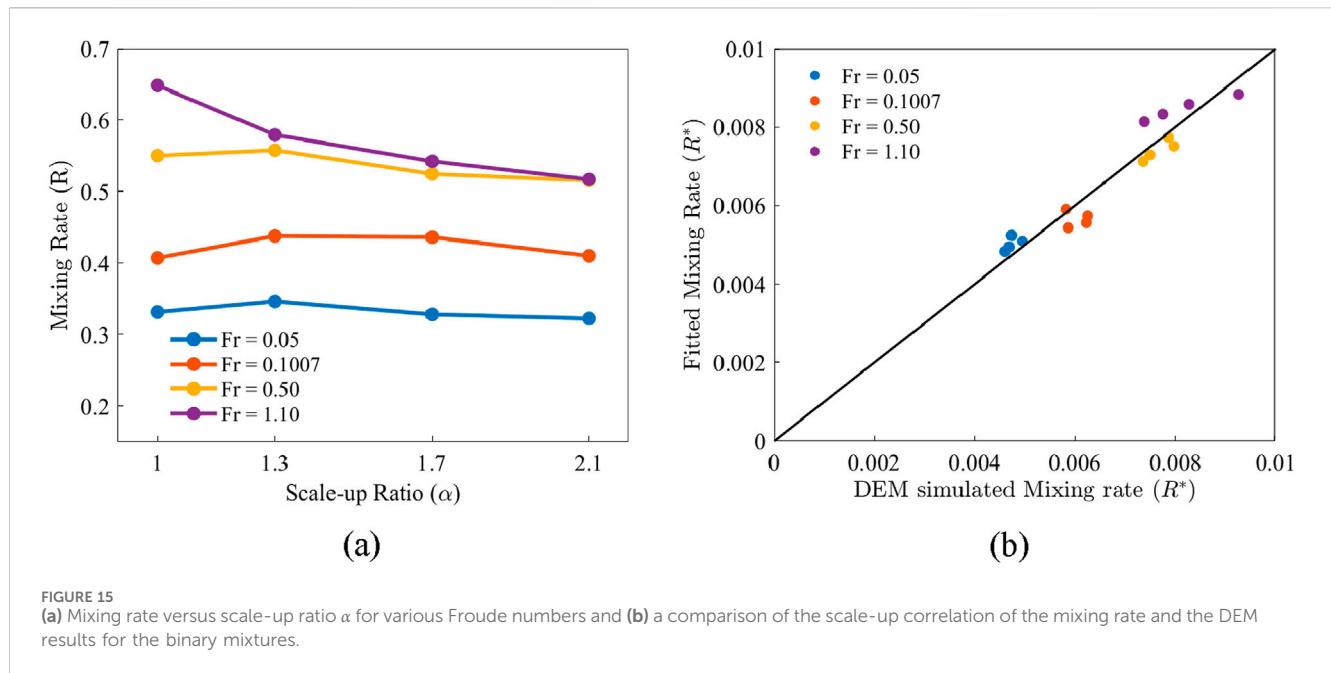


FIGURE 15
(a) Mixing rate versus scale-up ratio α for various Froude numbers and **(b)** a comparison of the scale-up correlation of the mixing rate and the DEM results for the binary mixtures.

like particles, indicating that particle shape has an impact on the scaling behavior.

- Average particle velocity increases as Froude number Fr and/or scale-up ratio α increase for both the monodisperse and binary systems, due to the increase in the boundary velocity of the drum.
- With increasing scale-up ratio α , the average contact force increases for the monodisperse systems while it changes non-monotonically at large Froude numbers for the binary systems.
- The mixing rate of the particles is significantly promoted by increasing Fr . The mixing rate maintains constant at small Fr and it decreases slowly with increasing α at large Fr , as it takes longer time for the particles to travel a longer distance to mix well globally in larger drums.
- The mixing index eventually achieves the same high level at various Froude numbers Fr for the monodisperse systems, while the final mixing indices are smaller at smaller Fr for the binary systems. In addition, it found that the mixing rate of the binary mixtures has a stronger dependence on the scale-up ratio α than the monodisperse systems.

This work provides some new results and primary insights on scale-up behaviors of flow and mixing of elongated particles. It is expected to be useful in the design of handling of non-spherical particles in rotating drums. In order to achieve a more comprehensive understanding of the scale-up rules, much larger scale-up ratios should be considered in the future work.

Data availability statement

The original contributions presented in the study are included in the article/supplementary material, further inquiries can be directed to the corresponding authors.

Author contributions

JS: Visualization, Methodology, Formal Analysis, Writing – review and editing, Writing – original draft, Software, Investigation. NN: Methodology, Visualization, Investigation, Validation, Software, Formal Analysis, Writing – original draft, Writing – review and editing. HF: Investigation, Visualization, Writing – review and editing, Formal Analysis. GL: Writing – review and editing, Formal Analysis, Investigation. ML: Writing – review and editing, Investigation, Formal Analysis. YG: Writing – review and editing, Methodology, Supervision, Formal Analysis. JL: Project administration, Supervision, Formal Analysis, Writing – review and editing. JT: Formal Analysis, Project administration, Methodology, Writing – review and editing, Supervision, Investigation.

Funding

The author(s) declare that no financial support was received for the research and/or publication of this article.

Conflict of interest

Authors JS, GL, and JT were employed by China Tobacco Zhejiang Industrial Co., Ltd. Authors HF and ML were employed by China Tobacco Zhejiang Industrial Co. Ltd.

The remaining authors declare that the research was conducted in the absence of any commercial or financial relationships that could be construed as a potential conflict of interest.

Generative AI statement

The author(s) declare that no Generative AI was used in the creation of this manuscript.

Publisher's note

All claims expressed in this article are solely those of the authors and do not necessarily represent those of their affiliated

organizations, or those of the publisher, the editors and the reviewers. Any product that may be evaluated in this article, or claim that may be made by its manufacturer, is not guaranteed or endorsed by the publisher.

References

- Alizadeh, E., Dubé, O., Bertrand, F., and Chaouki, J. (2013). Characterization of mixing and size segregation in a rotating drum by a particle tracking method. *AIChE J.* 59, 1894–1905. doi:10.1002/aic.13982
- Ardalani, E., Borghard, W. G., Glasser, B. J., and Cuitiño, A. M. (2023). Scale-up of heat transfer in a rotary drum equipped with baffles. *Powder Technol.* 429, 118879. doi:10.1016/j.powtec.2023.118879
- Beaulieu, C., Vidal, D., Niyonkuru, C., Wachs, A., Chaouki, J., and Bertrand, F. (2021). Effect of particle angularity on flow regime transitions and segregation of bidisperse blends in a rotating drum. *Comput. Part. Mech.* 9, 443–463. doi:10.1007/s40571-021-00421-1
- Bhalode, P., and Ierapetritou, M. (2020). A review of existing mixing indices in solid-based continuous blending operations. *Powder Technol.* 373, 195–209. doi:10.1016/j.powtec.2020.06.043
- Chen, G., Mei, Y., Zhang, Y., and Jin, B. (2024). DEM investigation on flow regime transition of cylindrical particle in a rotating drum. 22, 893, 912. doi:10.1515/ijcre-2024-0029
- Cui, X., Dai, J., Xu, H., and Gao, X. (2023). SuperDEM simulation and experiment validation of nonspherical particles flows in a rotating drum. *Ind. Eng. Chem. Res.* 62, 6525–6535. doi:10.1021/acs.iecr.3c00919
- Ding, Y. L., Forster, R. N., Seville, J. P. K., and Parker, D. J. (2001). Scaling relationships for rotating drums. *Chem. Eng. Sci.* 56, 3737–3750. doi:10.1016/S0009-2509(01)00092-6
- Dong, T., Yang, S., and Wang, S. (2024). Super-quadric DEM study of cylindrical particle behaviours in a rotating drum. *Powder Technol.* 437, 119511. doi:10.1016/j.powtec.2024.119511
- Figuroa, I., Vargas, W. L., and McCarthy, J. J. (2010). Mixing and heat conduction in rotating tumblers. *Chem. Eng. Sci.* 65, 1045–1054. doi:10.1016/j.ces.2009.09.058
- Govender, I. (2016). Granular flows in rotating drums: a rheological perspective. *Miner. Eng.* 92, 168–175. doi:10.1016/j.mineng.2016.03.021
- Gui, N., Yan, J., Xu, W., Ge, L., Wu, D., Ji, Z., et al. (2013). DEM simulation and analysis of particle mixing and heat conduction in a rotating drum. *Chem. Eng. Sci.* 97, 225–234. doi:10.1016/j.ces.2013.04.005
- Han, J., Shen, K., Guo, Y., Xiong, H., and Lin, J. (2023). Discrete element simulations of flexible ribbon-like particles. *Powder Technol.* 429, 118950. doi:10.1016/j.powtec.2023.118950
- He, J., Wang, Y., Yang, L., Zheng, Q., Xu, J., Liu, S., et al. (2024). Similarity analysis of size-induced segregation and flow behavior during the scaling up process of rotating drums. *Powder Technol.* 448, 120252. doi:10.1016/j.powtec.2024.120252
- He, S., Gan, J., Pinson, D., Yu, A., and Zhou, Z. (2020). A discrete element method study of monodisperse mixing of ellipsoidal particles in a rotating drum. *Ind. Eng. Chem. Res.* 59, 12458–12470. doi:10.1021/acs.iecr.9b06623
- Herman, A. P., Gan, J., and Yu, A. (2021). GPU-based DEM simulation for scale-up of bladed mixers. *Powder Technol.* 382, 300–317. doi:10.1016/j.powtec.2020.12.045
- Herman, A. P., Gan, J., Zhou, Z., and Yu, A. (2022a). Discrete particle simulation for mixing of granular materials in ribbon mixers: a scale-up study. *Powder Technol.* 400, 117222. doi:10.1016/j.powtec.2022.117222
- Herman, A. P., Zhou, Z., Gan, J., and Yu, A. (2022b). Scaling up studies for mixing of granular materials in rotating drums. *Powder Technol.* 403, 117408. doi:10.1016/j.powtec.2022.117408
- Jiang, C., An, X., Li, M., Wu, Y., Gou, D., and Wu, Y. (2023). DEM modelling and analysis of the mixing characteristics of sphere-cylinder granular mixture in a rotating drum. *Powder Technol.* 426, 118653. doi:10.1016/j.powtec.2023.118653
- Kodam, M., Curtis, J., Hancock, B., and Wassgren, C. (2012). Discrete element method modeling of bi-convex pharmaceutical tablets: contact detection algorithms and validation. *Chem. Eng. Sci.* 69, 587–601. doi:10.1016/j.ces.2011.11.011
- Kumar, S., Khatoon, S., Dubey, P., Yogi, J., and Anand, A. (2024). Shape-dependent radial segregation in rotating drum: insights from DEM simulations. *Powder Technol.* 432, 119134. doi:10.1016/j.powtec.2023.119134
- Lacey, P. M. C. (1954). Developments in the theory of particle mixing. *J. Appl. Chem.* 4, 257–268. doi:10.1002/jctb.5010040504
- Li, L., Kemp, I., and Palmer, M. (2020). A DEM-based mechanistic model for scale-up of industrial tablet coating processes. *Powder Technol.* 364, 698–707. doi:10.1016/j.powtec.2020.01.087
- Li, M., Wu, Y., Qian, Y., An, X., and Li, H. (2021). DEM simulation on mixing characteristics and macroscopic/microscopic flow behaviors of different-shaped spherocylinders in a rotating drum. *Ind. Eng. Chem. Res.* 60, 8874–8887. doi:10.1021/acs.iecr.1c00962
- Li, Y., You, Y., Gou, D., Yu, A., and Yang, R. (2022). A DEM based scale-up model for tumbling ball mills. *Powder Technol.* 409, 117854. doi:10.1016/j.powtec.2022.117854
- Liu, Z., Ma, H., Zhou, L., Xu, C., Zhang, X., and Zhao, Y. (2024). DEM-DDM investigation of the intra-tablet coating uniformity for tablets with different shapes. *Powder Technol.* 438, 119666. doi:10.1016/j.powtec.2024.119666
- Ma, H., Zhou, L., Liu, Z., Chen, M., Xia, X., and Zhao, Y. (2022). A review of recent development for the CFD-DEM investigations of non-spherical particles. *Powder Technol.* 412, 117972. doi:10.1016/j.powtec.2022.117972
- Miao, Q., Cao, Y., Zhu, W., Huang, P., Huang, L., Yu, A., et al. (2024). Segregation flow behavior of polydisperse particle mixture with skewed distribution in a rotating drum. *Powder Technol.* 444, 120041. doi:10.1016/j.powtec.2024.120041
- Norouzi, H. R., Zarghami, R., and Mostoufi, N. (2015). Insights into the granular flow in rotating drums. *Chem. Eng. Res. Des.* 102, 12–25. doi:10.1016/j.cherd.2015.06.010
- Orozco, L. F., Nguyen, D.-H., Delenne, J.-Y., Sornay, P., and Radjai, F. (2020). Discrete-element simulations of comminution in rotating drums: effects of grinding media. *Powder Technol.* 362, 157–167. doi:10.1016/j.powtec.2019.12.014
- Portillo, P. M., Ierapetritou, M., Tomassone, S., Mc Dade, C., Clancy, D., Avontuur, P. P. C., et al. (2008). Quality by design methodology for development and scale-up of batch mixing processes. *J. Pharm. Innovation* 3, 258–270. doi:10.1007/s12247-008-9048-9
- Rudge, J. F., Holness, M. B., and Smith, G. C. (2008). Quantitative textural analysis of packings of elongate crystals. *Contrib. Mineral. Petrol.* 156, 413–429. doi:10.1007/s00410-008-0293-1
- Trojcosky, M. (2019). Rotary drums for efficient drying and cooling. *Dry. Technol.* 37, 632–651. doi:10.1080/07373937.2018.1552597
- Vu, D. C., Amarsid, L., Delenne, J.-Y., Richefeu, V., and Radjai, F. (2024). Rheology and scaling behavior of polyhedral particle flows in rotating drums. *Powder Technol.* 434, 119338. doi:10.1016/j.powtec.2023.119338
- Xu, G., Zhang, Y., Yang, X., Chen, G., and Jin, B. (2023). Effect of drum structure on particle mixing behavior based on DEM method. *Particuology* 74, 74–91. doi:10.1016/j.partic.2022.05.008
- Yang, R. Y., Yu, A. B., McElroy, L., and Bao, J. (2008). Numerical simulation of particle dynamics in different flow regimes in a rotating drum. *Powder Technol.* 188, 170–177. doi:10.1016/j.powtec.2008.04.081
- Yang, S., Zhang, L., Luo, K., and Chew, J. W. (2017). DEM study of the size-induced segregation dynamics of a ternary-size granular mixture in the rolling-regime rotating drum. *Phys. Fluids* 29, 123301. doi:10.1063/1.5008297
- Yu, F., Zhang, S., Zhou, G., Zhang, Y., and Ge, W. (2018). Geometrically exact discrete-element-method (DEM) simulation on the flow and mixing of spherocylinders in horizontal drums. *Powder Technol.* 336, 415–425. doi:10.1016/j.powtec.2018.05.040
- Yu, F., Zhang, Y., Zheng, Y., Han, M., Chen, G., and Yao, Z. (2020). Comparison of different effective diameter calculating methods for spherocylinders by geometrically exact DEM simulations. *Powder Technol.* 360, 1092–1101. doi:10.1016/j.powtec.2019.10.097
- Zhu, H. P., Zhou, Z. Y., Yang, R. Y., and Yu, A. B. (2007). Discrete particle simulation of particulate systems: theoretical developments. *Chem. Eng. Sci.* 62, 3378–3396. doi:10.1016/j.ces.2006.12.089